

X-ray Spectral Study of the extended emission, 'the Cap', located 11.6 kpc above the disk of M82

Takeshi Go TSURU¹, Midori OZAWA¹, Yoshiaki HYODO¹, Hironori MATSUMOTO¹,
Katsuji KOYAMA¹, Hisamitsu AWAKI², Ryuichi FUJIMOTO³,
Richard GRIFFITHS⁴, Caroline KILBOURNE⁵, Kyoko MATSUSHITA⁶,
Kazuhisa MITSUDA³, Andrew PTAK⁷, Piero RANALLI⁸, and Noriko Y. YAMASAKI³

¹ *Department of Physics, Kyoto University, Sakyo-ku, Kyoto 606-8502*
tsuru@cr.scphys.kyoto-u.ac.jp, midori@cr.scphys.kyoto-u.ac.jp

² *Department of Physics, Ehime University, 2-5 Bunkyo, Matsuyama, Ehime 790-8577*

³ *ISAS/JAXA, 2-1-1 Yoshinodai, Sagamihara 229-8510*

⁴ *Department of Physics, Carnegie Mellon University, Pittsburgh, PA 15213, USA*

⁵ *NASA Goddard Space Flight Center, Greenbelt, MD 20771, USA*

⁶ *Department of Physics, Tokyo University of Science,*
Kagurazaka, Shinjuku-ku, Tokyo 162-8601

⁷ *Department of Physics and Astronomy, Johns Hopkins University,*
3400 N. Charles St., Baltimore, MD 21218, USA

⁸ *Cosmic Radiation Lab., RIKEN, 2-1 Hirosawa, Wako, Saitama 351-0198*

(Received 2006 August 10; accepted 2006 September 20)

Abstract

The extended X-ray emission from 'the Cap' region located 11' (11.6 kpc) above the disk of the starburst galaxy M82 has been observed with Suzaku and XMM-Newton. Owing to the good energy resolution and the large collecting area of the XIS on Suzaku, combined with similar properties of the EPIC instrument on XMM-Newton, we have clearly detected K-shell emission lines from O VII, O VIII, Ne X, Mg XI, Mg XII and the Fe-L complex. Two optically-thin thermal plasma components are required to fit the observed X-ray spectra. We have determined the metal abundances of O, Ne, Mg, Si and Fe in this region for the first time. Their metal abundance ratios agree well with those of metal-poor stars and the model prediction of metals synthesized by type-II supernovae, but they are not consistent with the metallicities of type-Ia supernovae. This result is support for the idea that the origin of the metals in the Cap is type-II supernovae explosions occurring in the starburst regions in the M82 galaxy. We discuss the possible contribution from sputtered dust grains to the metals in the Cap. An emission line consistent with the C VI transition of $n = 4$ to 1 at 0.459 keV is marginally detected, although it is not statistically significant at the 99% confidence level; the presence of this line would suggest charge-exchange processes in the Cap.

Key words: Galaxies: individual (M82) Galaxies: abundance X-rays: spectra

1. Introduction

Starbursts inject a large amount of kinetic and thermal energy into intergalactic space via outflows enriched with heavy metals synthesized in the massive stars that result in supernova explosions. The metal-enriched ejecta mix with the intergalactic medium and now form part of the warm-hot intergalactic medium (WHIM) and intra-cluster medium (ICM). Using ASCA results, Fukazawa et al. (1998), Finoguenov, David, Ponman (2000) and Finoguenov, Arnaud, David (2001) showed the importance of the metal enrichment of the ICM by type-II supernova activity in starbursts at early epochs. The entropy excess in the ICM above the self-similar prediction implies the importance of non-gravitational heating. One of the plausible heat sources is that from the superwinds which result from starbursts (Ponman, Cannon, Navarro 1999; Lloyd-Davies, Ponman, Cannon 2000). Thus, starburst activity is a key phenomenon when trying to understand the metal and thermal evolution of galaxies and clusters of galaxies. In spite of the fact that we cannot see the initial starbursts directly, the observation of hot plasma currently being produced by the nearby starburst galaxies can reveal the basic processes and give us insight into the same processes at high redshift.

Since M82 is a prototypical starburst galaxy and one of the brightest starburst galaxies in the local universe, it has been studied at almost all wavelengths, ranging from low frequency radio up to TeV γ -rays. Essentially all X-ray astronomical satellites have observed M82. The extended X-ray structure basically consists of a multi-phase thermal plasma extending from the nuclear region toward the halo, mainly along the minor axis of the galaxy (Watson,

Table 1. The numbers of atoms per a H atom for the solar metal abundances adopted in this paper (Anders, Grevesse 1989).

atom	number	atom	number	atom	number
He	0.0977	C	3.63×10^{-4}	N	1.12×10^{-4}
O	8.51×10^{-4}	Ne	1.23×10^{-4}	Mg	3.80×10^{-5}
Si	3.55×10^{-5}	S	1.62×10^{-5}	Ar	3.63×10^{-6}
Ca	2.99×10^{-6}	Fe	4.68×10^{-5}	Ni	1.78×10^{-6}

Stanger, Griffiths 1984; Fabbiano 1988; Strickland, Ponman, Stevens 1997). The point sources in M82 include the hyper luminous X-ray source, M82 X-1, dominating X-ray luminosity above ~ 3 keV (Matsumoto, Tsuru 1999; Ptak, Griffiths 1999; Matsumoto et al. 2001; Kaaret et al. 2001).

The spectral and spatial structure of the thermal plasma component of M82 has been vigorously studied with CCDs or IGSPCs onboard ASCA, BeppoSAX, Chandra and XMM-Newton (Moran, Lehnert 1997; Ptak et al. 1997; Tsuru et al. 1997; Cappi et al. 1999; Weaver, Heckman, Dahlem 2000; Griffiths et al. 2000; Stevens, Read, Bravo-Guerrero 2003; Ranalli et al. 2005). The results from the observation with RGS were reported by Read, Stevens (2002) and Origlia et al. (2004). The X-ray spectra are well represented by a model consisting of multiple thermal plasma components ($k_{\text{B}}T \sim 0.3 - 1.5$ keV) with absorption due to the cool matter in the M82 galaxy. The measurements of absolute metal abundances differ by a factor of several to ten among the measurements with ASCA, XMM-Newton/EPIC and RGS (Tsuru et al. 1997; Read, Stevens 2002; Stevens, Read, Bravo-Guerrero 2003; Origlia et al. 2004). The abundances of O and Fe are lower than those of Si and S by a factor of several, a common result from the ASCA and XMM-Newton/RGS observations. Any combination of the metal production of type-Ia and type-II supernovae cannot explain the abundance ratios among the metals. Recently, Ranalli et al. (2005) have reported that the metal abundances and their ratios significantly change from the nucleus toward the halo. Additionally, the Fe abundance of ~ 0.3 solar was obtained for the high temperature diffuse plasma in the core of M82 (Griffiths et al. 2000). Thus, the metal abundances of the X-ray plasmas in the M82 galaxy itself are still under debate.

Searching for very extended X-ray emission far beyond the halo of the M82 galaxy, Tsuru et al. (1990) have claimed evidence for X-ray emission extending for 100 kpc around M82 from scanning observations with the Ginga satellite. Extended emission named 'the Cap' in the $H\alpha$ and soft X-ray bands was discovered at approximately $11'$, corresponding to 11.6 kpc at the distance of 3.63 Mpc, to the north of the center of M82 (Devine, Bally 1999; Lehnert, Heckman, Weaver 1999). Comparing the $H\alpha$ and the X-ray morphology, Lehnert, Heckman, Weaver (1999) have revealed a close relationship between the two emissions. This X-ray emission has been confirmed with XMM-Newton by Stevens, Read, Bravo-Guerrero (2003). Lehnert, Heckman, Weaver (1999) explained its X-ray emission as the result of shock heating associated with an encounter between the starburst-driven galactic superwind and a large photoionized cloud in the halo of M82. Hoopes et al. (2005) detected UV emission at the Cap with GALEX and suggested that the most likely emission mechanism is scattering of stellar continuum from the starburst in M82 by dust in the Cap. The X-ray spectra of the Cap region obtained with ROSAT and XMM-Newton can be fitted with a thermal plasma model with a temperature of $k_{\text{B}}T = 0.80 \pm 0.17$ keV or $0.65^{+0.69}_{-0.62}$ keV (Lehnert, Heckman, Weaver 1999; Stevens, Read, Bravo-Guerrero 2003). The metal abundance of this plasma is key information in unraveling the origin and fate of the ejecta. However, no successful measurement has been made so far due to the limited spectral resolution and/or statistics.

Thus, we made a 109 ks observation of the Cap with the Suzaku XIS. The XIS has good energy resolution, especially in the low energy band from 0.3 to 1.0 keV, and low detector background. These properties have enabled us to obtain the best quality X-ray spectrum in the Cap region and to elucidate the nature of the plasma, and especially to measure the metal abundances. We also analyzed the archival data of the XMM-Newton observation of M82, in which the Cap was also observed in the same field of view. Throughout this paper, we adopt a distance of $D = 3.63$ Mpc to M82 (Freedman et al. 1990). The solar metal abundances adopted in this paper are shown in table 1.

2. Observation and Data Reduction

2.1. Data reduction of the Suzaku observation

Three pointing observations aimed at the region including M82 and the Cap were made with the X-ray CCD camera (XIS) onboard the Suzaku satellite in October 2005 during the phase reserved for the Science Working Group (the SWG phase). The details of the Suzaku satellite, the XRT and the XIS are found in Mitsuda et al. (2006), Serlemitsos et al. (2006) and Koyama et al. (2006), respectively. Data taken at an elevation angle less than 5° from the Earth rim or during the passage through the South Atlantic Anomaly were removed (Revision 0.7 data).

The reduction of the data from the 4 sensors of the XIS have been made with XSELECT version 2.3 as follows. Firstly, we removed the telemetry saturated data using GTI (good time interval) files. These GTI files were provided

Table 2. The logs of Suzaku and XMM-Newton observations of M82.

Instrument	Seq. No.	Observation Start Date	Effective Exposure
XIS	100033010	2005/10/04	36.8 ks
	100033020	2005/10/19	41.7 ks
	100033030	2005/10/27	30.5 ks
EPIC-pn	0206080101	2004/04/21	53.0 ks
EPIC-MOS	0206080101	2004/04/21	65.0 ks

by the XIS team through the Suzaku official web page¹. Secondly we removed hot and flickering pixels. Further, we did not use the data when the satellite attitude was not stable after manoeuvre procedures. We confirmed from the light curve that there were no data saturated periods during the observation. After the filters and reductions were applied, we confirmed that the data obtained from regions of blank sky showed no significant time variability.

We compiled the data from the 3x3 and 5x5 modes of the three observations into one. After these filters were applied, a net exposure time of 109 ks was left for both BI and FI. The observation logs are given in table 2.

2.2. Data reduction of the XMM-Newton observation

M82 and the Cap were observed twice with XMM-Newton. The details of the XMM-Newton satellite, the EPIC-MOS and pn instruments can be found in Jansen et al. (2001), Turner et al. (2001) and Strüder et al. (2001), respectively. The effective exposure after the screening of the first observation on 2001 May 6 was 20-30 ks (Read, Stevens 2002; Origlia et al. 2004; Stevens, Read, Bravo-Guerrero 2003). Out of the total exposure time of 100 ks in the second observation on 2004 April 21, an effective exposure of 59-65 ks was left, which is two or three times longer than that of the first one. The energy resolution of the EPIC-MOS was significantly improved after 2002 November by changing the detector temperature of EPIC from -100°C to -120°C (Kirsch et al. 2005). For these reasons, we concentrate on the second observation in this paper.

The data from the EPIC-MOS and pn instruments have been processed with the standard procedures of the XMM-Newton SAS (Science Analysis System 6.0.0). Periods of high background were filtered out, i.e. EPIC-MOS data with a counting rate above 0.3 counts s^{-1} in the energy band 10-15 keV were removed. As for the EPIC-pn, we did not use data with a counting rate above 1.0 counts s^{-1} in the same energy band. After these filters were applied, net exposures of 59 ks and 65 ks were left for the EPIC-MOS and pn instruments, respectively. The observation logs are also given in table 2.

3. Analysis and Results

3.1. Imaging Analysis and Overall Structure

Figures 1 and 2 show X-ray images of M82 in the energy band 0.3-2 keV obtained with Suzaku XIS1 (BI) and XMM-Newton MOS1+MOS2, respectively. The X-ray emission of the M82 galaxy in the energy band 3-10 keV is dominated by the hyper-luminous X-ray source M82 X-1 (Matsumoto, Tsuru 1999; Matsumoto et al. 2001). The nominal positions of the X-ray peak (henceforth 'M82 X-1') in the images in the energy band 3-10 keV obtained with Suzaku XIS and XMM-Newton EPIC-MOS are $(\alpha_{2000}, \delta_{2000}) = (9^{\text{h}}55^{\text{m}}47.0^{\text{s}}, 69^{\circ}40'07'')$ and $(9^{\text{h}}55^{\text{m}}50.6^{\text{s}}, 69^{\circ}40'45'')$, respectively. Another bright point source 'B' seen in the XIS image at $(9^{\text{h}}55^{\text{m}}11.5^{\text{s}}, 69^{\circ}46'55'')$ in the nominal Suzaku coordinates can be identified with a point source at $(9^{\text{h}}55^{\text{m}}14.8^{\text{s}}, 69^{\circ}47'36'')$ in the EPIC-MOS image. The absolute pointing accuracy of XMM-Newton is better than $1''$. Therefore, the Suzaku nominal coordinate system is systematically shifted by $(3.7^{\text{s}}, 39.5'')$ from the XMM-Newton coordinates. This spatial offset is within the calibration accuracy at the time of writing (Serlemitsos et al. 2006). Thus, we tuned the Suzaku coordinates by shifting $(-3.7^{\text{s}}, -39.5'')$.

Clear diffuse X-ray emission is seen in the Cap region of both figures 1 and 2, and this is the prime target of this paper. In the XMM-Newton image, a point source denoted as 'C' is detected at the position $(\alpha_{2000}, \delta_{2000}) = (09^{\text{h}}55^{\text{m}}27.7^{\text{s}}, +69^{\circ}52'1'')$, is consistent with the point source seen at $(09^{\text{h}}55^{\text{m}}29.6^{\text{s}}, +69^{\circ}51'55'')$ in the ROSAT observation (Lehnert, Heckman, Weaver 1999). This point source is identified with a stellar object having an R magnitude of 12.2 (Lehnert, Heckman, Weaver 1999). The source C is unclear in the Suzaku image of figure 1. As described in the following section, point source C has the low flux of $1.6 \times 10^{-14}\text{ ergs cm}^{-2}\text{ s}^{-1}$ in the energy band 0.3-3 keV, and is therefore too faint to be detected with Suzaku.

In addition to the X-ray emission at the Cap, diffuse X-ray emission is clearly seen in the connecting region between the Cap and the M82 galaxy (figures 1 and 2) as already reported by Stevens, Read, Bravo-Guerrero (2003). Our

¹ <http://www.astro.isas.jaxa.jp/suzaku/>

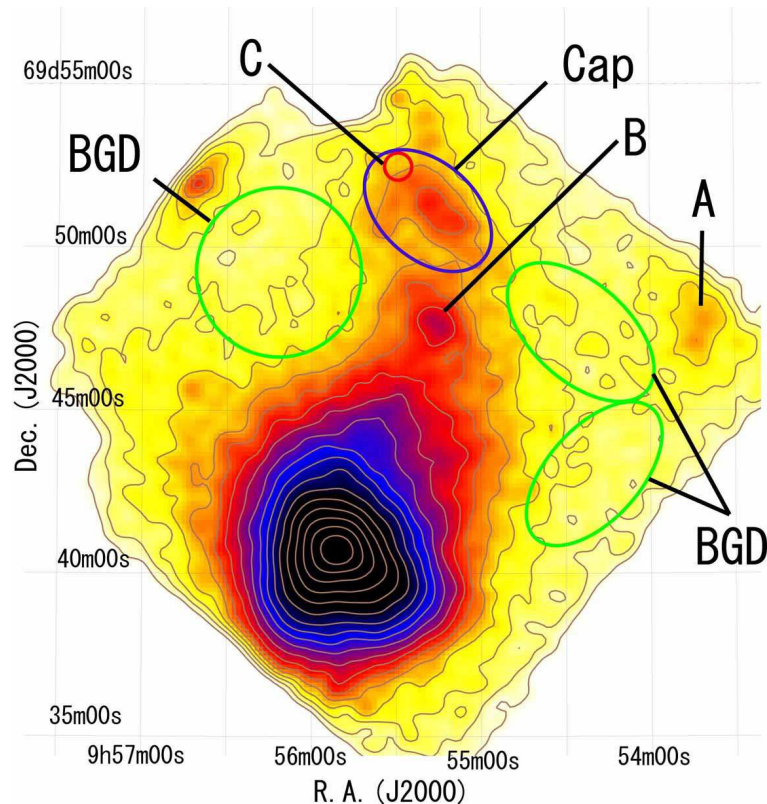


Fig. 1. X-ray image obtained with the Suzaku XIS1 (BI) in the energy band 0.3-2 keV. The attitude correction has been already done by comparison with the XMM-Newton/EPIC-MOS image. The image has been smoothed with $\sigma = 3$ pixels. The regions used for the spectra of the Cap and BGD are shown. The position of the sources A, B and C are also indicated.

preliminary analysis of the XMM-Newton data show that this diffuse emission has a flux of 8.9×10^{-14} ergs cm $^{-2}$ s $^{-1}$ in the energy band 0.3-3 keV.

We note that the source 'A' at $(\alpha_{2000}, \delta_{2000}) = (09^{\text{h}}53^{\text{m}}43.5^{\text{s}}, +69^{\circ}47'35'')$ is also a diffuse X-ray source. Gal et al. (2003) reported that a cluster of galaxies, NSC J095337+694751 at a red-shift of $z = 0.211$, is located at the position $(\alpha_{2000}, \delta_{2000}) = (09^{\text{h}}53^{\text{m}}37.53^{\text{s}}, +69^{\circ}47'50.9'')$. Source 'A' could therefore be identified with the cluster in spite of the separation of $\sim 0.6'$ between the two positions.

3.2. Spectrum Analysis of EPIC data of the Cap

We analyzed the EPIC-MOS and pn data for the Cap and a background area near the Cap, inside the bounding regions shown in figure 2. Before background subtraction, the total counts from the Cap region in the energy band 0.3-3 keV were 2496 and 3610 counts for the EPIC-MOS and pn, respectively. After subtraction of the background data, the flux from the Cap region was 1.2×10^{-13} ergs cm $^{-2}$ s $^{-1}$ in the energy band 0.3-3 keV. The background subtracted spectra are given in figure 3 along with the best fitted model spectra. The details of the spectral fits will be described in section 3.5.1.

3.3. Spectral Analysis of the EPIC data on Point Source C

The primary purpose of this paper is to obtain a high quality X-ray spectrum of the Cap. Because it is difficult to resolve point source C from the diffuse component of the Cap using the Suzaku XIS, we analyzed the EPIC data to obtain the spectrum of point source C. From the small region including point source C shown in figure 2, 268 and 402 counts were obtained for the EPIC-MOS and pn, respectively. No significant time variability was detected within the XMM-Newton exposure. After subtraction of the background data from the same region as that used for the Cap, the flux of source C was 1.6×10^{-14} ergs cm $^{-2}$ s $^{-1}$ in the same band. Thus, the flux of source C is 13% of that of the Cap, indicating that the contribution from this source is relatively minor in the whole Cap region.

We fitted the EPIC-MOS and pn spectra of point source C in the energy band 0.3-3 keV and obtained an acceptable result with an empirical model consisting of two thin thermal plasma components, in which we adopted the vMEKAL model incorporated in XSPEC version 11.3 (Mewe, Gronenschild, van den Oord 1985). The best fit parameters are given in table 3. Its thermal nature of the spectrum is consistent with a late-type dwarf star, which is suggested by

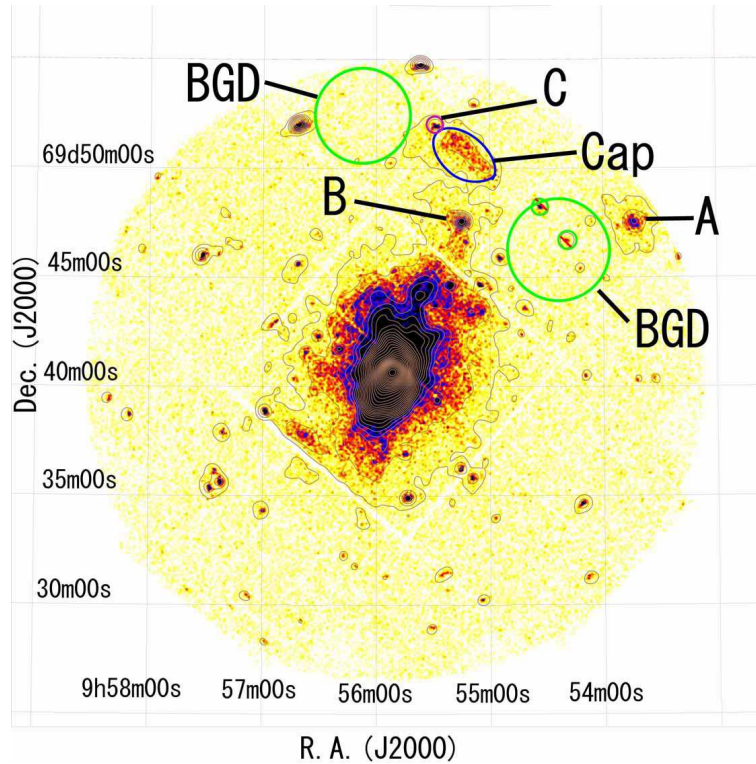


Fig. 2. X-ray image obtained with EPIC-MOS1 and MOS2 in the energy band 0.3-2 keV. The image is smoothed with $\sigma = 3$ pixels. The regions used for the spectra of the Cap and BGD are shown. The position of the sources A, B and C are also indicated. The data from the two small circles inside one of the BGD regions were not used because point sources are located there.

Lehnert, Heckman, Weaver (1999). This model spectrum describing point source C will be included in every spectral fit for the Suzaku spectra of the Cap in the following analysis.

3.4. Procedure used for the Spectral Analysis of the XIS data

Previous observations of the M82 galaxy showed that its X-ray spectrum is well described by a thermal plasma model, in which prominent thermal emission lines of several elements are detected (Tsuru et al. 1997; Ptak et al. 1997; Read, Stevens 2002; Stevens, Read, Bravo-Guerrero 2003). Thus, in order to check the XIS gain using these lines, we produced an X-ray spectrum for each XIS sensor by collecting counts within a circular region with a radius of 2.48 arcmin around M82. We used the versions of February 13, 2006 and May 28, 2006 for the response (RMF) and xissimarfgen (ARF) (Ishisaki et al. 2006), respectively. We detected prominent K emission lines of O VII, O VIII, Ne X, Mg XI and Mg XII in the spectra. We fitted these spectra with gaussian functions and a power law model empirically describing the emission lines and the continuum component. Comparing the center energies of the lines with the theoretical values, we found that the discrepancies are less than 4 eV, which indicates that the absolute energy scale of the XIS data is well calibrated.

The optical blocking filters (OBF hereafter) of the XIS sensors are unfortunately contaminated by outgas from the satellite (Koyama et al. 2006). The results from the XIS calibration show that the column density of the contaminant can be described as a function of the radial distance from the center of the XIS field of view (FOV). The vignetting of the XRT is also given as a function of radius from the FOV center (Serlemitsos et al. 2006). Thus, we selected the Cap and the BGD regions to have the same distance from the FOV center in order to reduce the systematic errors due to the calibration uncertainties from the contaminant and the vignetting function (figure 1). The ARFs are calculated with xissimarfgen on the assumption that the BGD and the Cap are uniformly diffuse and point like, respectively.

We performed background subtraction on the XIS spectra of the Cap with the two methods described below. The first one is a simple method in which we collected background spectra from the BGD region shown in figure 1 and subtracted them from the ones of the Cap (method 1). The background subtracted XIS FI and BI spectra of the Cap are shown in figure 4, where the FI data from the three instruments (XIS0, XIS2 and XIS3) are combined. Note that the spectra also include the contribution from point source C detected with XMM-Newton. Subtraction of a model spectrum for this source will be done during the spectral fitting for the Cap.

In the second method, we fitted spectra of the X-ray background and included this model in the fits to the X-ray spectra of the Cap as mentioned below (method 2). The model describing point source C is also included in the fitting.

In the first step of this method, we made spectra of the night earth data having the same detector coordinates as the Cap region and used these as the detector background. We adopted night earth data collected by the Suzaku XIS team from September 2005 to May 2006 and screened in the Revision 0.7 procedure. After the filters were applied, a net exposure time of 797 ks was left for both FI and BI detectors. We subtracted the spectra of the night earth (as the detector background) from those of the Cap. We followed the same procedure for the background region. Hereafter we call the night-earth-subtracted spectra of the Cap and background region 'the CAP-NTE' and 'the BGD-NTE', respectively.

The BGD-NTE is thought to consist of the cosmic X-ray background (CXB) and the soft X-ray background (SXB). To determine these components, we fitted the BGD-NTE spectra. The CAP-NTE spectra comprise the X-ray emission from the Cap, point source C, the CXB and the SXB, the last two of which can be determined with the BGD-NTE. Thus, we made spectral fits to the BGD-NTE using the model spectrum describing the CXB plus SXB. The model spectrum of point source C was already obtained in section 3.3. Including the models for the BGD-NTE and point source C in the fits for the CAP-NTE, we finally obtained the X-ray spectra of the Cap.

Then, if we were to adopt the best fit model for the BGD-NTE as the 'X-ray background' and use it in the spectral fit to the CAP-NTE, it would result in ignoring the statistical errors included in the observed spectra of BGD-NTE. Thus, we conducted simultaneous fits to the spectra of the CAP-NTE and the BGD-NTE linking the model parameters describing the X-ray background (the CXB and SXB) to be common in both of the fits. This method allows us to include the statistical errors of the CAP-NTE into the fit to the spectrum of the Cap as a contribution to the errors of the model parameters. In addition to the fits to the XIS spectra in the second method, we included the EPIC spectra of the Cap and made joint spectral fits in order to improve the overall fit. The results are given in the next section.

3.5. Results from the Spectral Analyses of the Cap

3.5.1. Using Simple Background Subtraction (method 1)

Figures 3 and 4 show the spectra of the Cap obtained with the EPIC and XIS with the best fit model spectra. In the XIS spectra of the Cap, several prominent K emission lines are seen and identified with O VII (0.57 keV), O VIII (0.65 keV), Ne X (1.02 keV), Mg XI (1.34 keV), Mg XII (1.47 keV) and the Fe-L complex. Stevens, Read, Bravo-Guerrero (2003) reported that the Cap spectra obtained with the first observation of XMM-Newton can be represented by a single thin thermal plasma model with the metal abundances fixed at the solar values. Therefore, we started fitting the XIS spectra with a single absorbed thin thermal plasma model with a temperature of $k_B T \sim 0.6$ keV plus the best-fit model for point source C. We used vMEKAL in XSPEC for the thermal plasma model (Mewe, Gronenschild, van den Oord 1985). The energy band above 3 keV was ignored, since no significant flux was detected there. With this fit, we did not reach reasonable results even when the metal abundances were left free, since a positive residual was found at O VII (1vMEKAL in table 3). We also found a positive residual at the O VII K emission line energy (0.57 keV) from the fit to the EPIC spectra with the same model, although the overall structure of the EPIC spectra is described well by a single thermal plasma model. The line emissivity of O VII at a temperature of $k_B T \sim 0.6$ keV is only $\sim 2\%$ of that at $k_B T \sim 0.17$ keV, which is the temperature giving the peak emissivity of the O VII line. Thus, this result suggests the need for an additional component to explain the O VII line.

Firstly, we fitted a thermal plasma model plus a narrow gaussian line to match the O VII line (1vMEKAL+1GAUS). We found that this gave a reasonable result, as shown in table 3. The center energy of the gaussian line is consistent with the theoretical value of O VII K emission at 0.57 keV. $\chi^2/\text{d.o.f.}$ is reduced from 503.2/361 for the 1vMEKAL model to 479.4/359 for 1vMEKAL+1GAUS, which allows us to conclude the introduction of 1GAUS is significant from the statistical point of view. However, the upper limit on the absorption column obtained from this fit contradicts the results from HI observations, as shown by the following argument. The column density of the cool matter in our galaxy toward the M82 region is $N_H = 4.0 \times 10^{20} \text{ cm}^{-2}$ (Dickey, Lockman 1990). The M81/M82 group are shown to be embedded in a large complex cloud of neutral H (Cottrel 1977; Appleton, Davis, Stephenson 1981). It has been shown that there is an apparent hole in the HI emission and thus the Cap region does not show any associated HI emission (Lehnert, Heckman, Weaver 1999; Stevens, Read, Bravo-Guerrero 2003). In fact, the column density of the HI cloud in the Cap region is less than $2.7 \times 10^{19} \text{ cm}^{-2}$ (Yun, Ho, Lo 1993; Yun, Ho, Lo 1994).

We have to take into account the contaminant on the XIS OBFs and its associated uncertainty. The column densities of the carbon contaminant on the OBFs at the XIS detector positions corresponding with the Cap observations is estimated to be 7.08×10^{17} , 8.01×10^{17} , 1.08×10^{18} and $2.15 \times 10^{18} \text{ cm}^{-2}$ for XIS0, XIS1, XIS2, and XIS3, respectively. The column densities of O are assumed to be 1/6 those of C. The thickness of the contaminant on the XIS OBFs still has some uncertainty, estimated to be $\pm 20\%$ at the time of writing (Koyama et al. 2006). In the energy band of 0.3-1 keV, the absorption due to the contaminant corresponds to the one due to HI with $N_H = 2.5 \times 10^{20} \sim 7.6 \times 10^{20} \text{ cm}^{-2}$. Thus, the uncertainty in the contaminant thickness is equivalent to a galactic absorption of $\Delta N_H = (0.5 \sim 1.5) \times 10^{20} \text{ cm}^{-2}$. Note that the uncertainty equivalent to the galactic absorption for XIS1 (BI) is $\Delta N_H = 0.5 \times 10^{20} \text{ cm}^{-2}$; this detector is the most sensitive to the absorption column. Even if the uncertainty on the contaminant is taken into account, the upper limit on the absorption column density derived from the spectral fit is still lower than that of the galactic HI. Thus, we conclude that the model of a thermal plasma plus a narrow gaussian line is physically inadequate for the

Table 3. The results from the simple background-subtracted spectra are described (method 1 in the text). The component normalization of the vMEKAL model is $(10^{-14}/4\pi D^2) \int n_H n_e dV \text{cm}^{-5}$, where V is the volume and D the distance. The metal abundances are given in units of the solar value. The abundances of the metals except the ones given in the table are fixed to be solar. The unit of absorption column is 10^{20}cm^{-2} . The normalization of the gaussian line is defined as an unabsorbed photon flux in units of $10^{-6} \text{ph cm}^{-2} \text{s}^{-1}$.

Data	point source 'C'		The Cap	
Instruments	EPIC		EPIC & XIS	
Model	2vMEKAL	1vMEKAL	1vMEKAL+1GAUS	2vMEKAL
N_H	0 (fixed)	< 1.43 (90%) < 2.54 (99%)	< 1.26 (90%) < 1.91 (99%)	< 6.4 (90%) < 9.0 (99%)
$k_B T$ (keV)	$0.28^{+0.05}_{-0.05}$	$0.63^{+0.02}_{-0.02}$	$0.63^{+0.02}_{-0.01}$	$0.21^{+0.06}_{-0.09}$
Norm.	2.66×10^{-6}	5.88×10^{-5}	5.27×10^{-5}	1.01×10^{-5}
$k_B T$ (keV)	$0.99^{+0.11}_{-0.16}$	$0.63^{+0.02}_{-0.02}$
Norm.	4.48×10^{-6}	4.51×10^{-5}
O	1 (fixed)	$1.18^{+0.27}_{-0.26}$	$1.33^{+0.11}_{-0.27}$	$1.15^{+1.00}_{-0.27}$
Ne	1 (fixed)	$0.84^{+0.31}_{-0.26}$	$0.99^{+0.28}_{-0.21}$	$1.31^{+0.43}_{-0.37}$
Mg	1 (fixed)	$1.17^{+0.31}_{-0.29}$	$1.37^{+0.28}_{-0.23}$	$1.81^{+1.02}_{-0.41}$
Si	1 (fixed)	$0.60^{+0.40}_{-0.36}$	$0.71^{+0.40}_{-0.38}$	$0.96^{+0.51}_{-0.48}$
Fe	1 (fixed)	$0.36^{+0.07}_{-0.06}$	$0.42^{+0.05}_{-0.03}$	$0.54^{+0.13}_{-0.07}$
LineE (keV)	$0.575^{+0.010}_{-0.016}$...
Norm.	$3.86^{+1.43}_{-1.16}$...
$\chi^2/\text{d.o.f.}$	22.55/22	503.2/361	479.4/359	478.2/359

description of the observed Cap spectra.

The above result is also evidence for the existence of an additional continuum component in the low-energy X-ray band. So we next tried a model consisting of two thin thermal plasma components (2vMEKAL) having common metal abundances, in which the lower temperature component explains the additional continuum component and the O VII line. The fit gave a satisfactory result, in which $\chi^2/\text{d.o.f.}$ of 2vMEKAL is nearly equal to that of 1vMEKAL+1GAUS (table 3). The upper limit on the column density of the absorbing cool matter is consistent with the sum of the column densities of the cool matter in our galaxy toward the M82 region ($N_H = 4.0 \times 10^{20} \text{cm}^{-2}$) and the upper limit on the column density of the HI cloud in the Cap region ($< 2.7 \times 10^{19} \text{cm}^{-2}$). In the following, we fix the whole absorption column density to be $N_H = 4.0 \times 10^{20} \text{cm}^{-2}$ in the fits.

3.5.2. Simultaneous Spectral Fitting of the Cap and the Blank Sky (method 2)

We now describe the results from the second method, employed with the purpose of improving the fit, in which simultaneous fits to the spectra of the CAP-NTE and the BGD-NTE were made.

Firstly, we fitted the BGD-NTE spectra. Specifically, we adopted an empirical X-ray background model consisting of two thin thermal plasma components and a power law component (2vMEKAL+POW). The former thermal components represent the soft X-ray background mainly due to the hot plasmas in our galaxy whereas the latter power law model fits the cosmic X-ray background (CXB) of extragalactic origin. The whole absorption was fixed at a column density of $N_H = 4.0 \times 10^{20} \text{cm}^{-2}$, which was described in section 3.5.1. We found that the model with the metal abundances fixed to solar values fails to represent the BGD-NTE spectra in the energy band of 0.3-7 keV. We therefore let the abundances of Ne, Mg, and Fe vary while the metal abundances were fixed to be common between the two thin thermal plasmas. This model gave a reasonable fit (table 4). The normalization and the photon index of the power law component are consistent with the values previously reported by Kushino et al. (2002) and Lumb et al. (2002).

Following the procedure described in section 3.4, we performed simultaneous fits to the XIS spectra of the CAP-NTE and the BGD-NTE. We also included the EPIC spectra obtained in section 3.5.1 in the fits. Since the X-ray spectrum of the Cap is soft, we used the data in the energy band 0.3-3 keV. The photon index of the CXB power law component was fixed to the best-fit values obtained above with the normalization left free, since we use the data only below 3 keV, where the contribution from the CXB is minor. The model spectrum describing point source C was fixed as before.

We first tried the model comprising a thermal plasma component and a narrow gaussian line explaining the O VII emission line, leaving the absorption column free (1vMEKAL+1GAUS). The results are given in table 4. We found the upper limit on the absorption column to be lower than that of our galaxy again, which confirms the conclusion obtained in section 3.5.1.

We next conducted the spectral fitting with two thermal plasma components (2vMEKAL). The whole absorption was fixed at a column density of $N_H = 4.0 \times 10^{20} \text{cm}^{-2}$ based on the results shown in section 3.5.1. The fit gave

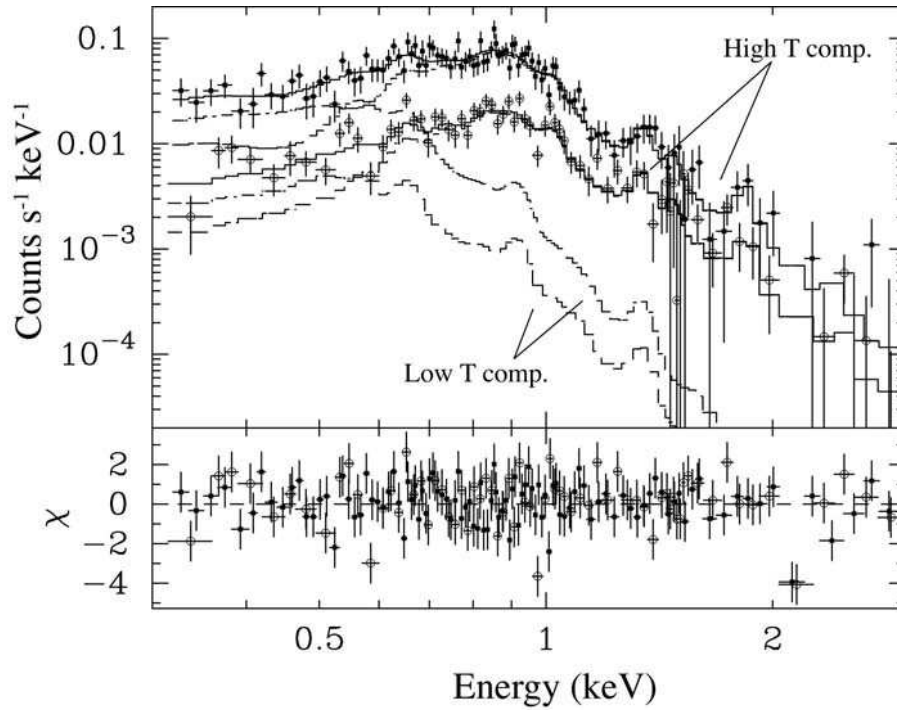


Fig. 3. The simple background-subtracted EPIC spectra of the Cap are shown with the best fit 2vMEKAL model spectra. Black squares indicate the EPIC-pn spectrum. The open circles show the combined spectrum of the two MOS (MOS1 and MOS2) with the normalization for one MOS sensor.

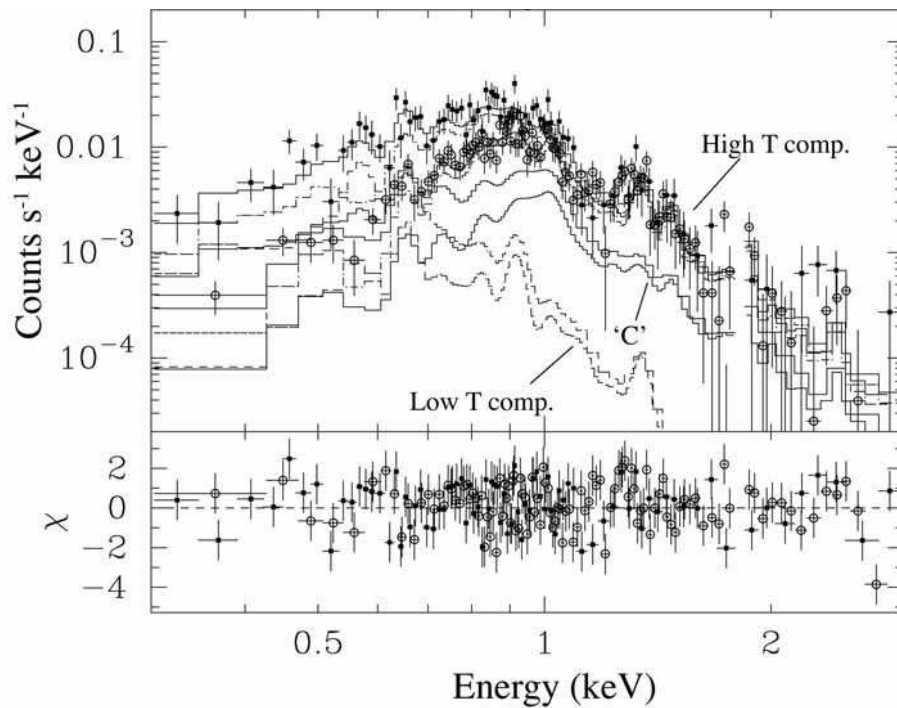


Fig. 4. The simple background-subtracted XIS spectra of the Cap are shown with the best fit 2vMEKAL model spectra. Black squares indicate the BI (XIS1) spectrum. The open circles show the combined spectrum of the three FI (XIS0,2,3) with the normalization for one FI sensor.

Table 4. The results from the simultaneous spectral fits to the Cap and the blank sky are described (method 2 in the text). Normalization for the fitting of 'BGD-NTE' is given for the actual BGD region shown in figure 1, where the ratio of BGD area to that of the Cap region is 4.34. The model component normalizations are: for the vMEKAL and vAPEC models $(10^{-14}/4\pi D^2) \int n_H n_e dV \text{cm}^{-5}$, where V is the volume and D the distance, while for the power-law model the unit of normalization is $\text{keV}^{-1} \text{cm}^{-2} \text{s}^{-1}$ at 1keV. The metal abundances are given in solar units. The abundances of the metals except the ones given in the table are fixed to be solar. The unit of absorption column is 10^{20}cm^{-2} . The normalization of the gaussian line is defined as an unabsorbed photon flux with a normalization unit of $10^{-6} \text{ph cm}^{-2} \text{s}^{-1}$.

Data	BGD-NTE		The Cap		
	2vMEKAL +1POW	1vMEKAL +1GAUS	2vMEKAL	2vAPEC	3vMEKAL
N_H	4 (fixed)	< 1.28 (90%) < 1.89 (99%)	4 (fixed)	4 (fixed)	4 (fixed)
$k_B T$ (keV)	$0.64^{+0.04}_{-0.04}$	$0.63^{+0.01}_{-0.01}$	$0.63^{+0.02}_{-0.02}$	$0.64^{+0.02}_{-0.02}$	$0.71^{+0.04}_{-0.08}$
Norm.	3.57×10^{-5}	6.18×10^{-5}	5.96×10^{-5}	6.22×10^{-5}	3.61×10^{-5}
$k_B T$ (keV)	$0.20^{+0.02}_{-0.02}$...	$0.20^{+0.01}_{-0.01}$	$0.23^{+0.03}_{-0.05}$	$0.13^{+0.08}_{-0.03}$
Norm.	3.85×10^{-5}	...	1.45×10^{-5}	2.48×10^{-5}	1.56×10^{-5}
$k_B T$ (keV)/ Γ	$1.27^{+0.09}_{-0.09}$	$0.44^{+0.10}_{-0.17}$
Norm.	4.26×10^{-5}	2.40×10^{-5}
O	1 (fixed)	$1.30^{+0.13}_{-0.18}$	$1.11^{+0.33}_{-0.32}$	$0.76^{+0.27}_{-0.20}$	$1.36^{+0.29}_{-0.47}$
Ne	$1.29^{+0.87}_{-0.68}$	$0.97^{+0.21}_{-0.19}$	$1.10^{+0.54}_{-0.40}$	$1.36^{+0.36}_{-0.40}$	$1.06^{+0.44}_{-0.44}$
Mg	$2.17^{+1.28}_{-0.77}$	$1.43^{+0.24}_{-0.22}$	$1.59^{+0.67}_{-0.48}$	$1.37^{+0.51}_{-0.36}$	$1.79^{+0.72}_{-0.56}$
Si	1 (fixed)	$0.92^{+0.37}_{-0.36}$	$1.03^{+0.58}_{-0.45}$	$0.86^{+0.43}_{-0.36}$	$1.15^{+0.61}_{-0.49}$
Fe	$0.51^{+0.24}_{-0.13}$	$0.42^{+0.03}_{-0.02}$	$0.49^{+0.07}_{-0.10}$	$0.44^{+0.08}_{-0.10}$	$0.54^{+0.08}_{-0.14}$
LineE (keV)	...	$0.570^{+0.003}_{-0.014}$
Norm.	...	$5.87^{+1.46}_{-1.63}$
$\chi^2/\text{d.o.f.}$	374.7/306	731.1/568	733.3/569	725.0/569	729.4/567

satisfactory results with nearly equal $\chi^2/\text{d.o.f.}$ to that of 1vMEKAL+1GAUS, consistent with the one obtained in section 3.5.1 while the errors of the parameters became smaller (table 4).

3.6. Uncertainty due to the Plasma Codes

The spectra obtained with XIS and EPIC show that the emission originates in two thermal plasma components. We first discuss the reliability of the results. We first tried the two-temperature vAPEC model (2vAPEC) for the fitting of the spectra instead of vMEKAL (Smith et al. 2001). The reduced χ^2 are almost the same between the two models. The temperatures, absolute metal abundances and their ratios agree with each other within the statistical errors although the absolute metal abundances obtained with the 2vAPEC model are somewhat lower than those with the 2vMEKAL model, except for Ne. Thus, there is no obvious reason for adopting one or other of the two models. Following the previous spectral studies of M82 and the Cap (Read, Stevens 2002; Stevens, Read, Bravo-Guerrero 2003; Origlia et al. 2004), we consider the adoption of vMEKAL as the plasma model in this paper.

3.7. Uncertainty due to the Contaminant on the OBF of the XIS sensors

As already mentioned, the thickness of the contaminant on the XIS OBFs still has some uncertainty at the time of writing (Koyama et al. 2006). The uncertainty of the column density of the contaminant affects the effective area in the soft energy band mainly below ~ 1 keV. In order to check its impact on the determination of the temperatures and metal abundances, we conducted spectral fits with 2vMEKAL by changing the thickness of the contaminant by $\pm 20\%$. The fit gave acceptable results. We found no change ($< 0.1\%$) in the temperature of the high plasma temperature component. The temperature of the low plasma temperature component varied by $\pm 5\%$, which is comparable with the statistical errors. The absolute metal abundances were affected at the level of $\pm 9\%$ (O), $\pm 2\%$ (Ne), $\pm 2\%$ (Mg), $\pm 1\%$ (Si) and $\pm 2\%$ (Fe), all of which are significantly smaller than the statistical errors. Thus, we conclude that the uncertainties due to the contaminant is generally negligible compared with the statistical errors. We note that nothing affects the value of the high temperature component because an X-ray spectrum with a temperature of $k_B T \sim 0.6$ keV is line dominated; hence the temperature determination is driven by the line energies, particularly the Fe-L centroid.

3.8. Uncertainty due to the Number of Thermal Components

The spectral analyses above show that two thermal plasma components are required to represent the observed spectra of XIS and EPIC. This would imply that the plasma of the Cap consists essentially of multi-components. Thus, one would suspect that the results from the spectral fits would be significantly affected by increasing the number of thermal components.

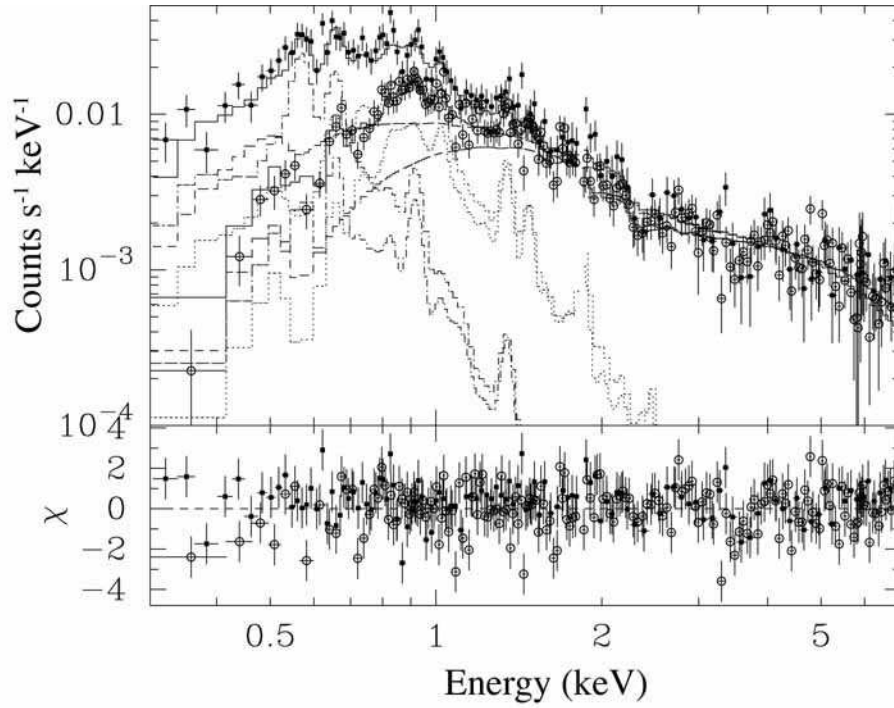


Fig. 5. The XIS spectra of 'BGD-NTE' are shown with the best fit model spectra. Black squares and open circles indicate the BI (XIS1) spectrum and the sum of the three FI (XIS0,2,3) spectra respectively. The normalization is given for one sensor.

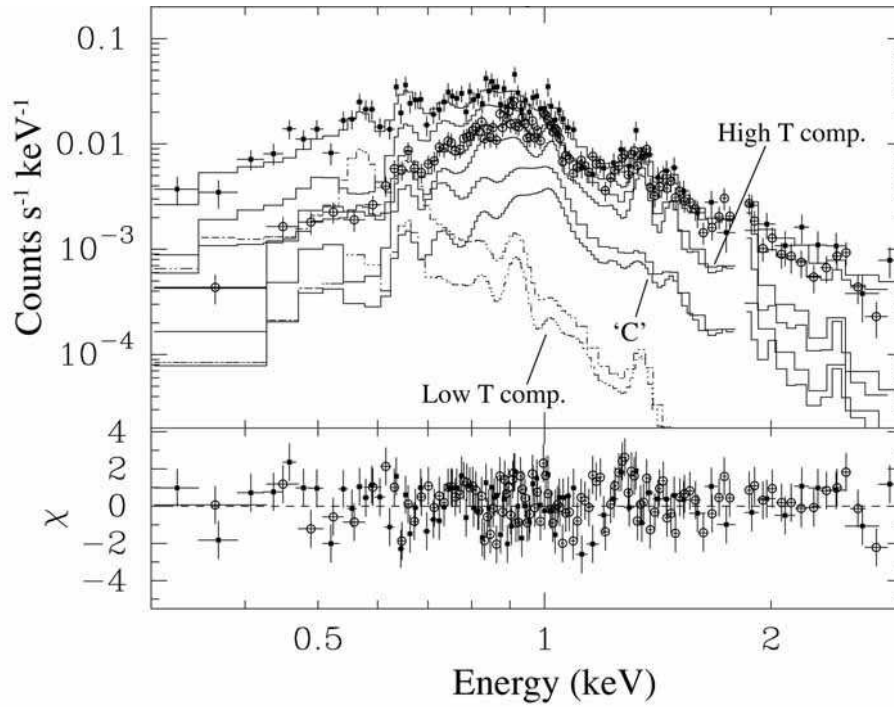


Fig. 6. The XIS spectra of 'CAP-NTE' are shown with the best fit model spectra of the two thermal plasma components of the Cap. Black squares and open circles indicate the BI (XIS1) spectrum and the combined spectrum of the three FI (XIS0,2,3), respectively. The normalization is given for one sensor.

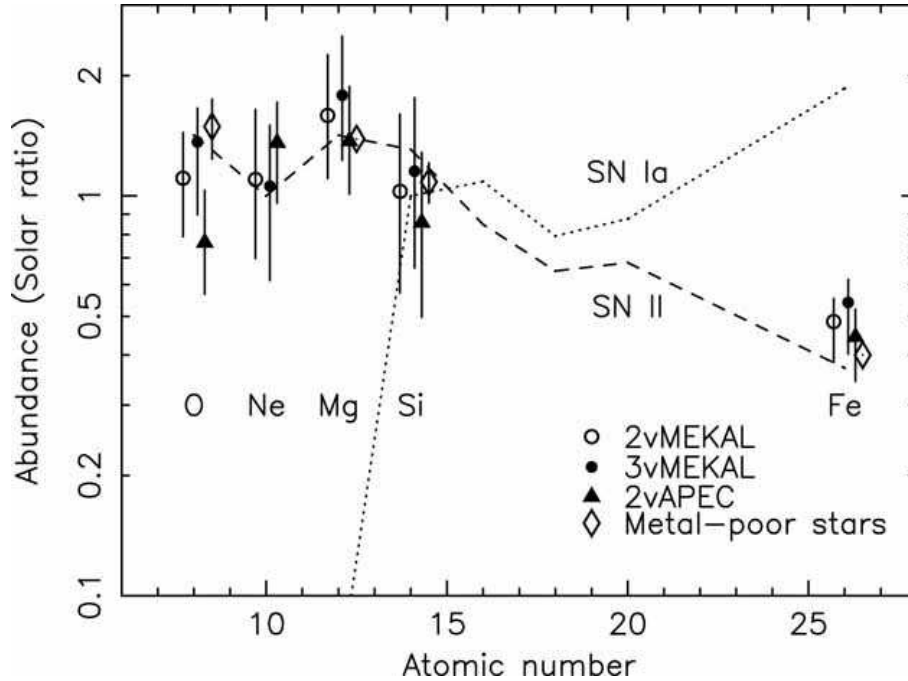


Fig. 7. Metal Abundances as a function of atomic number derived from the spectral fits. The dotted and dashed lines show the abundance ratios among metals synthesized by type-Ia and II supernovae, respectively. The average metal abundance ratios of metal-poor stars are also given, with the normalization such that the Fe abundance is 0.4 solar.

In order to check this, we made a fit with a model consisting of three plasma components (3vMEKAL) and found resulting temperatures of $k_B T = 0.13, 0.44$ and 0.71 keV (table 4). The reduction of χ^2 is only 3.9 against the number of the additional free model parameters of 2, meaning the introduction of the third component is not significant from the statistical point of view. The temperature and emission integral of the component with $k_B T = 0.13$ keV are consistent with those of the low temperature component of the two-temperature model within the statistical errors. In the three-component model, the sum of the emission measures and the weighted mean temperature with the emission integrals of the medium and high temperature components are almost the same as those of the high temperature component of the two-component model. The absolute metal abundances obtained with the three-component model are slightly higher than those of the two-component model (figure 7). Nevertheless, the differences between the two models are within the statistical errors.

In spite of the fact that the model consisting of a single thermal component plus a narrow gaussian line was physically rejected, its resulting metal abundances are also consistent with those with the 2vMEKAL model within the statistical errors (table 4). The derived temperature is consistent with that of the main component obtained in the two-temperature model. Thus, we can safely conclude that the results on the metal abundances and temperatures are robust even if the plasma of the Cap consists of single or multi components.

3.9. Non-Equilibrium Ionization

In the section 3.5.1, we argued that O VII K emission line is not explained by a single thermal plasma model with the temperature of $k_B T \sim 0.6$ keV well describing the overall structure of the observed spectra. It is because the only a small fraction of O stays in the ionization state of O VII for the temperature of $k_B T \sim 0.6$ keV in the equilibrium ionization. Thus, the K emission line from the relatively low ionization state of O VII might suggest the plasma is in a non-equilibrium ionization state.

In order to investigate it, we made a spectral analysis with a non-equilibrium ionization model with the simultaneous fitting to the Cap and the blank sky (method 2). We adopted the version 2.0 of the vNEI model incorporated in XSPEC version 11.3 (Borkowski, Sarazin, Blondin 1994; Borkowski, Lyerly, Reynolds 2001; Hamilton, Chevalier, Sarazin 1983; Liedahl, Osterheld, Goldstein 1995) and fixed the whole absorption column density to be $N_H = 4.0 \times 10^{20} \text{ cm}^{-2}$. The metal abundances of O, Ne, Mg, Si and Fe were left free as in the previous sections.

Figure 8 shows the confidence contour map for the ionization timescale (nt) as a function of the electron temperature ($k_B T$) in the 1vNEI model. We obtained the lower limit of $8.5 \times 10^{11} \text{ s cm}^{-3}$ on the ionization timescale at the 99% confidence level, which suggests the observed spectra is essentially consistent with an equilibrium ionization state. The significant positive residual at 0.57 keV consistent with the O VII K emission line was detected again. Thus, it leads

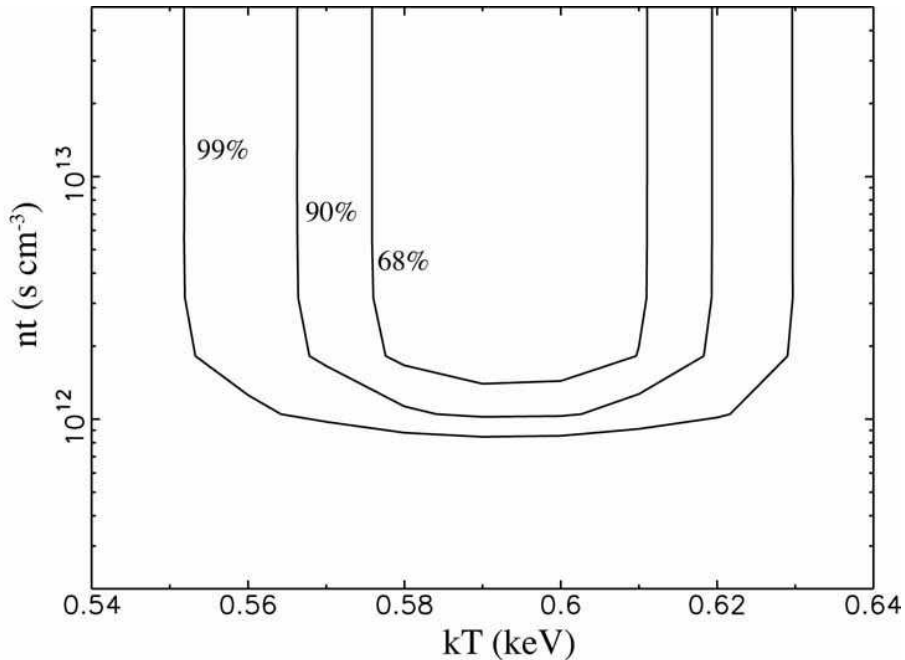


Fig. 8. The confidence contour map of the electron temperature (kT) and the ionization timescale (nt) obtained from the fitting with 1vNEI. The ionization time scale is defined in an unit of s cm^{-3} . The contours are given in confidence levels of 68%, 90% and 99%.

us to conclude that the model of a non-equilibrium ionization plasma dose not explain the O VII K emission line and the other spectral structures at the same time.

4. Discussion

4.1. Metal Abundance Ratios

Using the XIS and EPIC data, we demonstrated that the X-ray plasma of the Cap region consists of two thermal components. The high temperature component has $k_{\text{B}}T = 0.63 \pm 0.02$ keV, which agrees with the previously reported ones of $k_{\text{B}}T = 0.80 \pm 0.17$ keV and $k_{\text{B}}T = 0.65^{+0.04}_{-0.03}$ keV (Lehnert, Heckman, Weaver 1999; Stevens, Read, Bravo-Guerrero 2003). The emission integral of this component is also consistent with other observations. The existence of the O VII emission line and the low temperature component with $k_{\text{B}}T = 0.2$ keV is a new finding of this paper. It would reflect the nature of the plasma in the Cap region. However, we do not go into details in this paper.

The XIS image shows the existence of diffuse emission in the connecting region between M82 and the Cap (figure 1), as already pointed out by Stevens, Read, Bravo-Guerrero (2003). This may be expected from a large number of sequential supernovae, mostly type-II as a result of starburst activity occurring in M82. Thus, one would expect that the X-ray plasma in the Cap originates from the type-II supernovae in M82, a hypothesis which can be tested with the pattern of relative ratios of the metal abundances.

Thanks to the large effective areas and good energy resolution of the XIS and EPIC in the soft X-ray band, we successfully derived the metal abundances of O, Ne, Mg, Si and Fe in the X-ray plasma of the Cap for the first time. The abundances of O, Ne, Mg and Si are $1 \sim 2$ solar, while that of Fe is about 0.5 solar, which is generally consistent with the idea of the plasma originating from type-II supernovae. The emissivities of the lines depend on the plasma temperature, determined by the shape of the Fe L line complex, suggesting that the abundances obtained might be strongly coupled with the Fe abundance. Therefore, we have checked the reliability of the results. Figure 9 shows the confidence contours for the measured abundances of O, Ne, Mg and Si against Fe. This shows that the metal abundance ratios of O, Ne and Mg to Fe are higher than unity in units of the solar abundance, at a confidence level of 99%. An abundance ratio of unity between Si and Fe is permitted at a confidence level of 99%, but still rejected at the level of 90%. Thus, it is safely concluded that the Fe abundance is significantly lower than the others.

We have compared the metal abundance ratios of the Cap with those synthesized by type-II and type-Ia supernovae (figure 7). We adopted the W7 model in Nomoto, Thielemann, Yokoi (1984) and Thielemann, Nomoto, Yokoi (1986) for the metal masses synthesized by type-Ia supernovae. The model plot for type-Ia supernovae normalized with the Si abundance at the solar value shows clear disagreement with our observational result. This result is easily expected

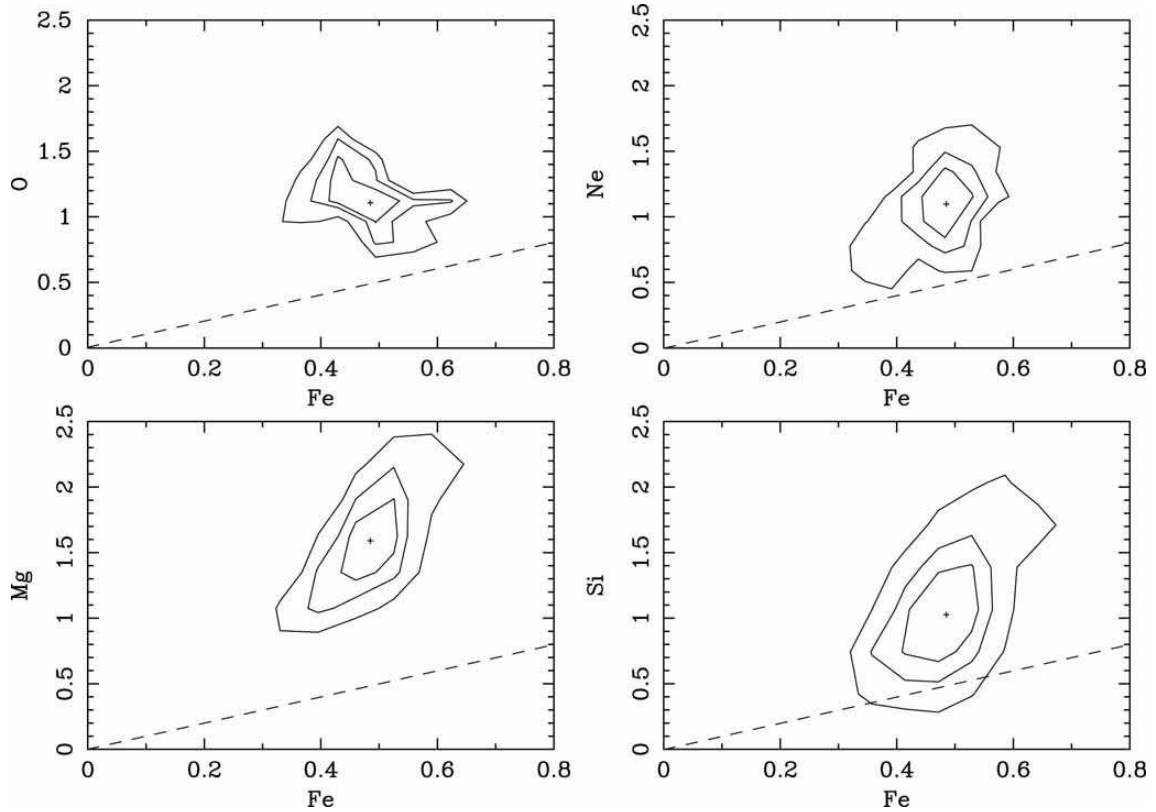


Fig. 9. The confidence contours for the O, Ne, Mg and Si abundances relative to the Fe abundance, obtained from the fits using the 2vMEKAL model. The contours are given at confidence levels of 68%, 90% and 99%. The dashed lines show the solar abundance ratio between the metals.

since O, Ne or Mg are not synthesized by type-Ia supernovae, while the metal abundances actually observed are much higher than that of Fe.

For type-II supernovae, we used the results of $m_u = 50 M_\odot$ by Tsujimoto et al. (1995), in which the averages of the synthesized masses are 1.8, 0.23, 0.12, 0.12, 0.041, 0.0080 and 0.0091 M_\odot for O, Ne, Mg, Si, S, Ar and Fe, respectively. We plot the metal abundance ratios synthesized by type-II supernovae, normalized with the Ne abundance at the solar value, in figure 7. Comparison with our results shows that metal synthesis by type-II supernovae agrees well with the observed metal abundance ratios in the Cap.

Another good (experimental) sample for metal synthesis by type-II supernovae comes from observations of metal-poor stars; these observations are free from the ambiguities resulting from the different supernova models. The chemical composition of these old stars reflects that of the gas from which they formed in the early universe, where type-II supernovae dominated type-Ia. Table 6 in Clementini et al. (1999) shows the average metal abundance ratios in metal-poor stars obtained with Hipparcos and ground-based observations. After the adjustment of the definition of the solar abundance, the metal abundance ratios relative to Fe in metal-poor stars are 3.1 ~ 4.4, 3.5 and 2.4 ~ 3.0 for O, Mg and Si, respectively. Figure 7 shows that the metal abundance ratios of the metal-poor stars and the Cap agree well with each other. Note that the absolute metal abundances of the metal-poor stars in the figure are meaningless since they are normalized so that the abundance of Fe is 0.4 solar.

Thus, the results of the comparison with models of type-II supernovae and metal-poor stars are consistent with the idea that the X-ray plasma in the Cap originates from type-II supernovae. On the other hand, type-Ia supernovae are not a major contributor to the metals in the Cap. Thus, this naturally leads to the suggestion that most of the metals ejected by M82 are synthesized by type-II supernovae occurring through its starburst activity.

4.2. Comparison with the Mass of the Dust in the Cap

Hoopes et al. (2005) detected UV emission at the Cap with GALEX. They suggest that the most likely UV emission mechanism is scattering of stellar continuum from the starburst in M82 by dust in the Cap. They also argue that the dust may have been pushed out of M82 by the starburst, or stripped from either M82 or M81 by the tidal interaction between the two galaxies. The former picture is supported by the SCUBA observation showing the outflowing dust from M82 (Alton, Davis, Bianchi 1999). The Spitzer result by Engelbracht et al. (2006) preferentially supports the

latter assumption.

Taking the composition of dust grains into account, Si and/or Fe with significant masses could exist in the form of dust in the Cap. Since the mass of the dust is not reported by Hoopes et al. (2005), it is impossible to make direct comparison between the metal masses in the X-ray plasmas and those in the dust at the moment. An upper limit on the HI column density of $2.7 \times 10^{19} \text{ cm}^{-2}$ is given by Yun, Ho, Lo (1993) and Yun, Ho, Lo (1994). Adopting a volume of $3.7 \times 3.7 \times 0.9 \text{ kpc}^3$ for the emission region of the Cap following Lehnert, Heckman, Weaver (1999), the upper limit on the mass of the HI cloud is $\sim 7 \times 10^5 M_\odot$. Assuming a gas-to-dust ratio of 100, the upper limit on the dust mass is $\sim 7 \times 10^3 M_\odot$.

Dust grains are sputtered in an X-ray plasma with a time scale of $t_{\text{sp}} \sim 10^8 (a/0.1 \mu\text{m}) (n/10^{-3} \text{ cm}^{-3})^{-1} \text{ yr}$ (Yamada, Kitayama 2005), where a and n are the size of the dust grains and the density of the plasma, respectively, where f_x is the filling factor. Estimating $n \sim 5 \times 10^{-3} \text{ cm}^{-3} \cdot f_x^{-0.5}$, the sputtering time scale is $t_{\text{sp}} \sim 2 \times 10^7 \text{ yr} \cdot f_x^{0.5}$. This is comparable with the travel time scale of $\sim 1.5 \times 10^7 \text{ yr}$ from M82 to the Cap at the shock speed of $\sim 740 \text{ km s}^{-1}$, where this speed is required to produce the plasma with $k_B T \sim 0.63 \text{ keV}$, following the estimation in Lehnert, Heckman, Weaver (1999). This suggests that some fraction of the dust grains have been possibly sputtered and mixed into the X-ray plasmas.

The masses of Si and Fe in the plasma phase obtained with our observation are $1.4 \times 10^3 \cdot f_x^{0.5} M_\odot$ and $1.8 \times 10^3 \cdot f_x^{0.5} M_\odot$, respectively, where f_x is the filling factor. The sum of these masses is comparable with the upper limit on the mass of the dust. Thus, it would seem possible that the dust could contribute a significant part of the metals in the X-ray plasmas. In other words, dust depletion due to sputtering could have an impact on the measured abundances from our X-ray results. Quantitative observation of the dust is crucial to understanding the ejecta from starburst activity and its fate. Further analyses and observations of the dust in the UV and submillimeter bands are very important.

4.3. Line Emission through The Charge-Exchange Process

Lallement (2004) has pointed out that the charge-exchange process could be important in X-ray line emission from the Cap, where the ionized superwind from M82 can be assumed to collide with cool ambient gas located at the Cap, as suggested by Lehnert, Heckman, Weaver (1999). The charge-exchange process contributes only emission lines to the X-ray spectrum. However, we have detected continuum emission in the observed X-ray spectra of the Cap. This observational result suggests that charge-exchange is not the major process in the Cap, although a minor contribution cannot be denied.

According to the charge-exchange emission model for comets by Krasnopolsky, Greenwood, Stancil (2004), the $n = 4$ to 1 transition line is enhanced for C VI at 0.459 keV. During the charge-exchange process, the electron from the donor neutral atom is first trapped at high levels, typically $n = 4$ for carbon. The Suzaku and XMM-Newton spectra given in figures 4, 6 and 3 show a hint of an emission line around 0.46 keV. Thus, we added a narrow gaussian line around 0.459 keV to the 2vMEKAL model and examined its confidence. Figure 10 shows the confidence contour map for the narrow gaussian line. A local minimum is found at an energy consistent with 0.459 keV, which suggests marginal detection of the C VI emission line although it is not statistically significant at the 99% confidence level.

We have estimated possible contributions to emission lines, especially O, due to the charge-exchange process. Following the model of Lehnert, Heckman, Weaver (1999), we again assume a box with dimensions of $3.7 \times 3.7 \times 0.9 \text{ kpc}^3$ for the Cap. An upper limit of $2 \times 10^{-3} \text{ cm}^{-3}$ has been obtained for the density of the HI cloud at the Cap (Yun, Ho, Lo 1993; Yun, Ho, Lo 1994). Thus, the upper limit on the column density of the HI cloud along the direction of the superwind from M82 is estimated to be $8 \times 10^{18} \text{ cm}^{-2}$. Since the cross-section of the charge-exchange between an O ion and a H atom is $\sim 10^{-15} - 10^{-14} \text{ cm}^2$ (Wegmann et al. 1998), it is expected that an O ion in the superwind would encounter a HI cloud thick enough for the charge-exchange process.

In this paper, we will not discuss the details of the process by which the superwind and O ions collide with the HI cloud. Nevertheless, we can estimate an upper limit on the photon flux of O emission lines assuming an extreme case in which all O ions suffer the charge-exchange process with HI and emit O K emission lines. Assuming a density of $\sim 1 \times 10^{-3} \text{ cm}^{-3}$, the velocity of the superwind of $\sim 740 \text{ km s}^{-1}$ and solar abundance of O in the plasma, the upper limit on the photon flux is estimated to be $5 \times 10^{-6} \text{ ph cm}^{-2} \text{ s}^{-1}$. The observed unabsorbed photon flux of O VII is $\sim 6 \times 10^{-6} \text{ ph cm}^{-2} \text{ s}^{-1}$ (tables 4). We note that the same logic gives an upper limit of $2 \times 10^{-6} \text{ ph cm}^{-2} \text{ s}^{-1}$ on the photon flux of C due to the charge-exchange process, and this is consistent with the upper limit on the one possible C VI emission line at 0.459 keV. Thus, the upper limit on the photon flux of the O K emission lines due to charge-exchange is at the same order of the one actually observed. This suggests that the charge-exchange process may make a significant contribution to the observed O K emission lines.

We thus expect that the charge-exchange process could be one of the key aspects of the understanding of the physical processes and the measurement of the metal abundances in the Cap, and hence the ejecta from starburst galaxies and its cosmic evolution. More extensive studies of the possible charge-exchange are definitely necessary. This could not be achieved with the limited spectral resolution of X-ray CCDs. The realization of the non-dispersion type of

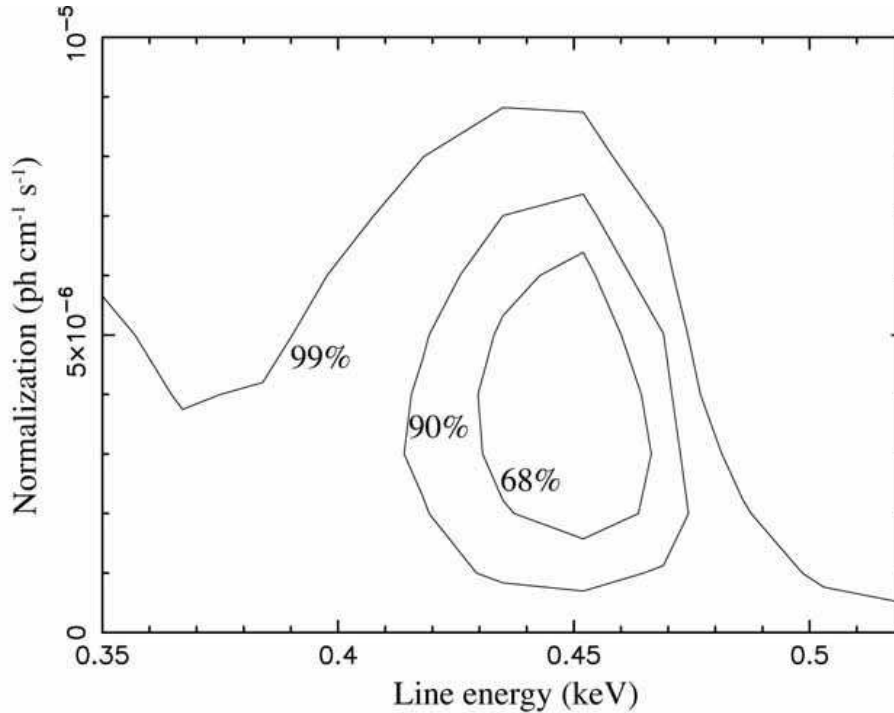


Fig. 10. The confidence contour map of the C VI emission line energy at 0.459 keV and its normalization obtained from the fitting with 2vMEKAL + 1GAUS. The normalization of the line is defined as an unabsorbed photon flux, where the normalization unit is $\text{ph cm}^{-2} \text{s}^{-1}$. The contours are given in confidence levels of 68%, 90% and 99%.

spectrometer with ultra high spectral resolution, i.e. the μ -calorimeters onboard the NeXT and DIOS missions is essential (Kunieda, Mitsuda, Takahashi 2006; Ohashi et al. 2006).

5. Summary

1. The Suzaku XIS clearly detected the diffuse X-ray emission from the Cap region located $\sim 11'$ to the north of the M82 galaxy. Additional diffuse X-ray emission is also detected in the connecting region between the Cap and the M82 galaxy.
2. The X-ray spectrum of the Cap is well described by a model with two thermal plasma components. The fit using the single-temperature model plus a narrow gaussian line at 0.57 keV is physically rejected because it resulted in a lower absorption column than that of our galaxy. Non-equilibrium ionization is not required to fit the spectra.
3. The metal abundance ratios of the Cap agree well with those of metal-poor stars and the model predictions of metals synthesized by type-II supernovae, but are not consistent with the models of type-Ia supernovae. This result supports the idea that the origin of the metals in the Cap is type-II supernovae explosions occurring in the starbursts in the M82 galaxy.
4. A significant contribution to the metals in the X-ray plasma in the Cap is possible from the sputtered grain dusts. This depends on the total mass of the dust.
5. An emission line consistent with the C VI transition from $n = 4$ to 1 at 0.459 keV is marginally detected. Although this is not statistically significant, it supports possible charge-exchange processes in the Cap. The charge-exchange process may also make a significant contribution to the observed O K emission lines.

Acknowledgement

We are grateful to all the members of the Suzaku hardware and software teams and the science working group. YH are supported by JSPS Research Fellowship for Young Scientists. REG acknowledges the support of NASA grant NNG05GR02G. This work is based by the Grant-in-Aid for the 21st Century COE "Center for Diversity and

Universality in Physics” from Ministry of Education, Culture, Sports, Science and Technology (MEXT) of Japan, and is supported on a Grant-in-aid (Fiscal Year 2002-2006) for one of Priority Research Areas in Japan; “New Development in Black Hole Astronomy”. This work is partially supported by Grants-in-Aid of Ministry of Education, Culture, Sports and Technology (MEXT) of Japan No. 15340088.

References

- Anders, E., & Grevesse, N., 1989, *Geochim. Cosmochim. Acta*, 53, 197
- Alton, P.B., Davis, J.I. & Bianchi, S., 1999, *A&A* 343, 51
- Appleton, P.N., Davis, R.D. & Stephenson, R.J., 1981, *MNRAS* 195, 327
- Borkowski, K.J., Sarazin, C.L., Blondin, J.M., 1994, *ApJ* 429, 710
- Borkowski, K.J., Lyerly, W.J., Reynolds, S.P., 2001, *ApJ* 548, 820
- Cappi, M. et al. 1999, *A&A* 350, 777
- Clementini, G., Gratton, R.G., Carretta, E., Sneden, C. 1999, *MNRAS* 302, 22
- Cottrel, G.A. 1977, *MNRAS* 178, 577
- Devine, D. & Bally, J., 1999, *ApJ* 510, 197
- Dickey, J.M. & Lockman, F.J., 1990, *ARA&A* 28, 215
- Engelbracht, C.W., et al. 2006, *ApJL* 642, L127
- Fabbiano, G., 1988, *ApJ* 330, 672
- Finoguenov, A., David, L.P., Ponman, T.J. 2000, *ApJ*, 544, 188
- Finoguenov, A., Arnaud, M., David, L.P., 2001, *ApJ*, 555, 191
- Freedman, W.L., et al., 1994, *ApJ* 427, 628
- Fukazawa, Y., et al., 1998, *PASJ* 50, 187
- Gal, R.R., et al., 2003, *AJ* 125, 2064
- Griffiths, R.E., et al. 2000, *Science* 290, 1325
- Hamilton, A.J.S., Chevalier, R.A., Sarazin, C.L., 1983, *ApJS* 51, 115
- Hoopes, C.G., et al., 2005, *ApJL* 619, L99
- Ishisaki, Y. et al., 2006, *PASJ* in press.
- Jansen, F., et al., 2001, *A&A* 365, L1
- Kirsch, M.G.F., et al. 2005, *SPIE* 5898, 224
- Kaaret, P. et al. 2001, *MNRAS* 321, L29
- Koyama, K. et al. 2006, *PASJ* in press.
- Krasnopolsky, V.A., Greenwood, J.B., Stancil, P.C., 2004, *Space Sci. Rev.*, 113, 271
- Kunieda, H., Mitsuda, K., Takahashi, T., 2006, *Proc. SPIE*, 6266, in press.
- Kushino, A., Ishisaki, Y., Morita, U., Yamasaki, N.Y., Ishida, M., Ohashi, T., & Ueda, Y., 2002, *PASJ* 54, 327
- Lallement, R., 2004, *A&A* 422, 391
- Liedahl, D.A., Osterheld, A.L., Goldstein, W.H. 1995, *ApJ* 438, 115
- Lloyd-Davies E.J., Ponman, T.J., & Cannon, D.B., 2000, *MNRAS* 315, 689
- Lehnert, M.D., Heckman, T.M., & Weaver, K.A., 1999, *ApJ* 523, 575
- Lumb, D.H., Warwick, R.S., Page, M., & De Luca A., 2002, *MNRAS* 389, 93
- Matsumoto, H. & Tsuru, T.G., 1999, *PASJ* 51, 321
- Matsumoto, H. Tsuru, T.G., Koyama, K., Awaki, H., Canizares, C.R., Kawai, N., Matsushita, S. & Kawabe, R., 2001, *ApJL* 547, L25
- Mewe, R., Gronenschild, E.H.B.M., & van den Oord, G.H.J., 1985, *A&AS* 62, 197
- Mitsuda, K. et al., 2006, *PASJ* in press.
- Moran, E.C., & Lehnert, M.D., 1997, *ApJ* 478, 172
- Nomoto, K., Thielemann, F.-K., Yokoi, K., 1984, *ApJ* 286, 644
- Ohashi, T. et al. 2006, *Proc. SPIE*, 6261, in press.
- Origlia, L., Ranalli, P., Comastri, A., & Maiolino, R., 2004, *ApJ* 606, 862
- Ponman, T.J., Cannon, D.B., & Navarro J.F., 1999, *Nature* 397, 135
- Ptak, A., Serlemitsos, P., Yaqoob, T., and Mushotzky, R., 1997, *AJ* 113, 1286
- Ptak, A., Griffiths, R., 1999, *ApJL* 517, L85
- Ranalli, P., et al. 2005, *Astro-Ph/051102*
- Read, A.M., & Stevens, I.R., 2002, *MNRAS* 335, L36
- Serlemitsos, P. et al. 2006, *PASJ* in press.
- Smith, R.K., Brickhouse, N.S., Liedahl, D.A. Raymond, J.C., 2001, *ApJL* 556, L91
- Stevens, I.R., Read, A.M., & Bravo-Guerrero, J., 2003, *MNRAS* 343, L47
- Strickland, D.K., Ponman, T.J., & Stevens, I.R., 1997, *A&A* 320, 378
- Strüder, L., et al., 2001, *A&A* 365, L18
- Thielemann F.-K., Nomoto, K., Yokoi, K., 1986, *A&A* 158, 17
- Turner, M.J.L., et al., 2001, *A&A* 365, L27
- Tsuru, T., et al., 1990, *PASJ* 42, L75
- Tsuru, T.G., Awaki, H., Koyama, K., & Ptak, A., 1997, *PASJ* 49, 619
- Tsujimoto, T, et al., 1995, *MNRAS* 277, 945
- Watson, M.G., Stanger, V., & Griffiths, R.E., 1984, *ApJ* 286, 144
- Weaver, K.A., Heckman, T.M., & Dahlem, M., 2000, *ApJ* 534, 684
- Wegmann, R., et al. 1998, *Planet. Space Sci.* 46, 603
- Yamada, K. & Kitayama, T., 2005, *PASJ* 57, 611
- Yun, M.S., Ho, P.T.P., & Lo, K.Y., 1993, *ApJL* 411, L17
- Yun, M.S., Ho, P.T.P., & Lo, K.Y., 1994, *Nature* 372, 530